Relationship of Microstructure to Properties of HIP and Weld Clad Alloy 625 in Sour Environments

W.J. SISAK*, RAGHAVAN AYER**+, R.R. MUELLER**, and D.P. LETA**

* Exxon Production Research Company, P.O. Box 2189, Houston, TX 77525-2189
**+ Presently with STEM, Inc., 305 Bic Drive, Milford, CT 06460
** Exxon Research and Engineering Company, Route 22 E, Annandale, NJ 08801

ABSTRACT

A study of the clad alloy 625 deposited by HIP and weld overlay on 4130 and 2¼Cr-1Mo steels was conducted to evaluate the effect of cladding process on microstructure, mechanical, corrosion and stress corrosion cracking (SCC) properties relating to sour gas production service. The results showed that the microstructure of the clad and interface produced by the two cladding processes are considerably different and had a direct effect on the properties. The clad produced by HIP had a homogenous structure which showed superior resistance to pitting, hydrogen disbond and SCC. In contrast, the HIP process resulted in a high concentration of coarse carbides resulting in poor mechanical properties of the clad/steel interface properties than in the weld clad. The segregated cast structure of the weld overlay alloy 625 contributed to the reduced resistance to corrosion and SCC of the weld clad compared to HIP clad. The weld clad interface also had fewer carbides which provided good mechanical integrity. Analysis of the microstructural characteristics and properties of the two clad materials are presented.

I. INTRODUCTION

There has been an increasing interest and need to optimize the cost and performance of materials considered for use in the production of hot sour gas reservoirs[1,2]. Therefore, cladding of nickel alloys to carbon steels is one of the options in materials selection. A typical use of clad steels in the production of oil and gas is as valves associated with wellheads, where a combination of strength and resistance to corrosion, stress corrosion cracking (SCC), and hydrogen embrittlement (HE) are required. Two commonly used cladding processes, weld overlay and Hot Isostatic Pressing (HIP), were considered for the wellhead application. Since the heat treatment and microstructures of clad Alloy 625 produced by the two processes are significantly different, determination of their suitability for use in sour environments requires a careful investigation[3]. In this paper, we characterize the microstructures produced by

Superalloys 718, 625 and Various Derivatives
Edited by Edward A. Loria
The Minerals, Metals & Materials Society, 1991

both types of cladding and relate the findings to their mechanical and corrosion properties.

II. EXPERIMENTAL PROCEDURE

II. A. Cladding Procedure

For weld cladding, steel valve bodies are machined oversized and heat treated for mechanical properties prior to cladding. Overlay processes typically utilize low heat input to minimize dilution of the clad layer with iron from the base steel. Following application of the weld overlay, the components are given a stress relief anneal and subsequently machined to final dimensions.

The HIP clad process uses heat and high pressure to metallurgically bond Alloy 625 to steel. Alloy 625 powder is added to specially designed steel cans that are positioned inside the component body which is machined oversized. The powder is consolidated into a fully-dense layer and bonded to the steel during the HIP cycle. HIP consists of an exposure in an inert gas environment at 1422 to 1477K at over 69 MPa isostatic pressure. Following HIP, the component is austenitized and tempered to obtain the required mechanical properties.

The clad samples for the present study were provided in the fully heat treated condition. The chemical composition of the clad layers produced by weld overlay and HIP are listed in Table I. The heat treatments for the clad materials which precede and follow the cladding process are listed in Table II. Heat treatment temperatures were chosen so as to achieve a 413 MPa yield strength for the 4130 steel and 517 MPa yield for the 2$_{1/4}$Cr-1Mo steel[a]. The material used for this study was taken from test pieces that were clad and heat treated by the same procedures used to manufacture weld overlay and HIP clad production components.

II. B. Microstructural Analysis:

The microstructural study determined the phase transformations at the interfaces of carbon steel/Alloy 625 clads using microanalytical methods consisting of x-ray microanalysis and Convergent Beam Electron Diffraction (CBED) in the transmission electron microscope (TEM), Scanning Electron Microscopy (SEM) and Secondary Ion Mass Spectroscopy (SIMS)[4]. Microstructures of the base clad layers, were also characterized.

II. C. Mechanical and Corrosion Properties:

The study of the mechanical and corrosion properties of the clad consisted of two parts: (i) evaluation of the integrity of the clad/steel interface, and (ii) evaluation of the environmental resistance of the clad layer. Interface tests evaluated resistance to both mechanical and hydrogen disbond while the environmental tests studied the

---

[a] Steel compositions conform with AISI specifications

pitting, crevice corrosion, SCC and HE resistance of the Alloy 625 clad. The specimens used for the mechanical disbond test and charging set-up for the hydrogen disbond test are shown in Figure 1. The Charpy-type specimens for mechanical disbond tests were notched such that the notch was oriented across the clad and base steel and crack propagation during testing occurred simultaneously in the clad and base steel. The hydrogen disbond test consisted of charging the clad at a current density of $10mA/cm^2$ followed by examination of the interface by Ultrasonic inspection (UT) and metallographic evaluation for formation of cracks. UT was also conducted on clads prior to hydrogen charging to document preexisting defects. Detailed procedure of the disbond tests are described elsewhere[5].

Pitting and crevice corrosion of the clad layers were measured following the procedure of ASTM G-48. The test solution contained 6 WT% $FeCl_3$, as in G-48, with an additional 10 WT% NaCl. The specimens were 25mm x 50mm x 6mm in size and were machined entirely from the clad layer within 0.5mm of the clad/steel interface. Artificial crevices were introduced using TFE fluorocarbon blocks which were fastened to the coupons with TFE tape. Coupons were immersed in the test solution at 298K for 72 hours, removed, rinsed and weighed. If no pits were observed, the specimens were returned to a new test solution and the solution temperature was increased; the procedure was repeated to a final temperature of 353K.

SCC and HE resistance were measured using slow strain rate tensile (SSRT) tests. Specimens were machined entirely from the clad layers of the test pieces and pulled to failure in uniaxial tension at a constant extension rate of 10^{-7} meters per second. The solution for SCC resistance consisted of 25 WT% NaCl and 0.5 WT% acetic acid in deionized water under a pressure of 0.69MPa H_2S gas. The test temperature was varied from 298 to 477K. The test solution for HE resistance was 25 WT% NaCl, saturated with H_2S gas at atmospheric pressure and 300K.

III. RESULTS

III. A. Microstructural Analysis

A detailed description of the microstructures resulting from cladding is presented in a recent publication[4] and only a brief summary is provided here. Microstructural features of both 4130 and 2¼Cr-1Mo steel clads were comparable, except for small differences which related to the difference in their carbon concentrations. In the following sections a general description of the microstructures is presented and relevant differences between the steels are indicated where appropriate.

III.A.1. Weld Clad:

Figure 2 shows a set of SEM micrographs from the base 4130 steel, interface region, and Alloy 625 weld. Two interesting microstructural features were observed in the TEM analysis of the interface. At the interface between the face-centered cubic austenite and the body-centered cubic ferrite, a thin zone of untempered martensite was observed to form almost continuously throughout the interface, Figure 3. The thickness of the martensite region varied in the range of 0.2 to 0.5 μm. In addition to

TABLE I
Chemical Analysis of Clad Layer from
Clad Test Blocks (WT.%)

	Ni	Cr	Mo	Nb + Ta	Ti	Al	C	P	S	Si	Fe
Weld	63.8	21.4	7.9	3.2	0.26	0.21	0.02	0.008	0.001	0.06	3.1
HIP	65.2	21.8	8.0	3.3	0.30	0.18	0.04	0.010	0.009	0.06	1.09

TABLE II
Heat Treatments for Weld- and HIP-Clad Spools

Weld-Clad		HIP-Clad	
4130 Base Steel	2-1/4 Cr -1 Mo Steel	4130 Base Steel	2-1/4 Cr -1 Mo Steel
N - 1172 K/4 hours, AC	N - 1227 K/15 hours, AC	Clad at 1394 K/4 hours, AC	Clad at 1394 K/4 hours, AC
A- 1130 K/4 hours, WQ	A - 1200 K/15 hours, WQ	N - 1172 K/3 hours, AC	N - 1227 K/1hour, AC
T - 933 K/6 hours, AC	T - 877 K/15 hours, WQ	A - 1144 K/3 hours, WQ	A - 1200K/1 hour, WQ
625 clad (gas-metal arc welding)	625 clad (gas-metal arc welding)	T - 936 K/3 hours, AC	T - 930 K/4 hours, WQ
SR - 936 K/3 hours, AC	SR - 947 K/3 hours, AC	--	T - 916 K/4 hours, WQ

KEY:
T = Temper N = Normalize A = Austenitize
SR = Stress Relief AC = Air Cool WQ = Water Quench

TABLE III
Crevice Corrosion and Pitting Resistance
of Weld- and HIP-Clad Inconel 625

Test Condition: 72 hour exposures in aqueous solution of a 6% $FeCl_3$ and 10% NaCl.

	Exposure Temperature						
Material	297 K	324 K	329 K	336 K	343 K	349 K	353 K
Weld-Clad 625	O	C	C	C	C	C	C,P
HIP-Clad 625	O	O	O	O	C	C	C

O - No Crevice C- Crevice Corrosion P - Pitting

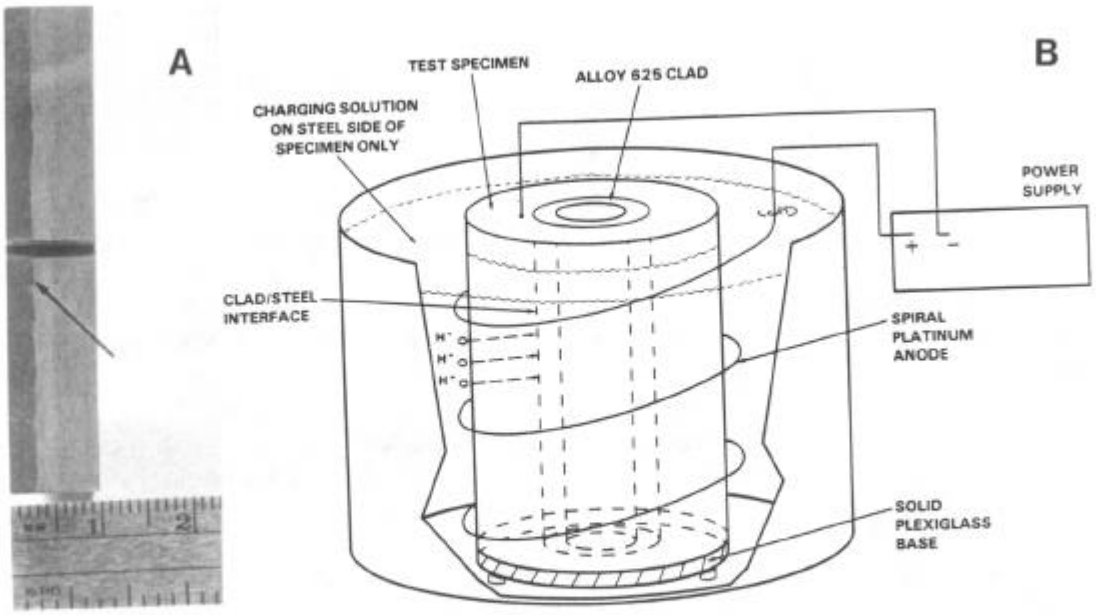

Figure 1: (a) Charpy sample for the mechanical disbond test; arrow indicates interface, and (b) charging set-up for hydrogen disbond test.

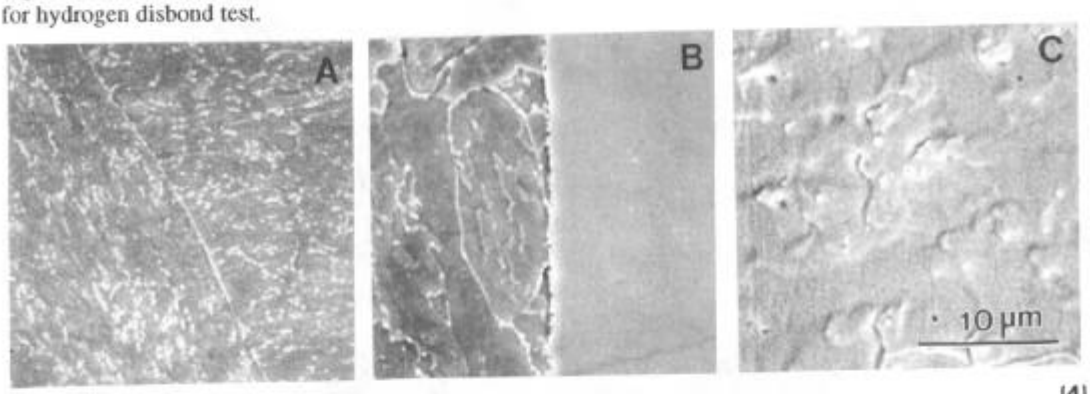

Figure 2: SEM images of weld clad showing microstructures of (a) steel, (b) interface, and (c) IN626 clad.[4]

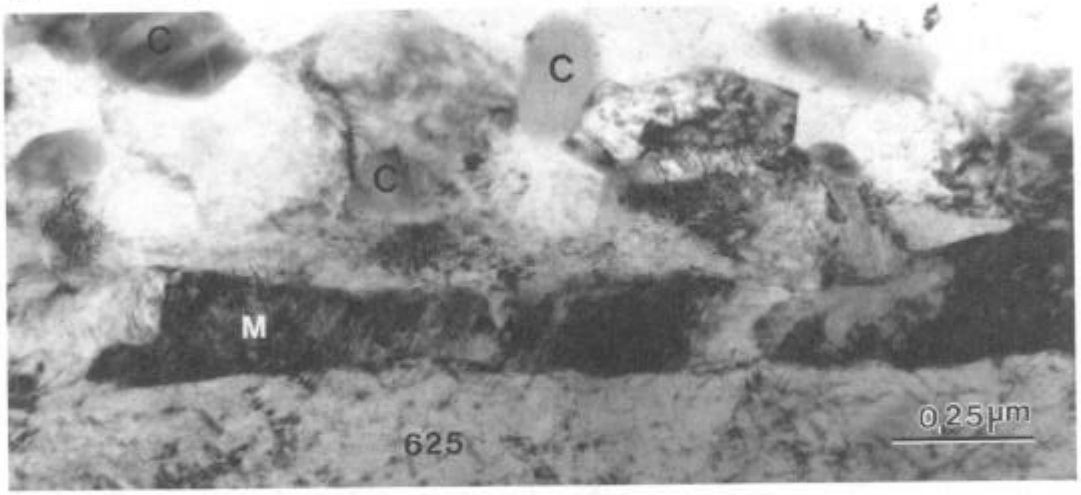

Figure 3: TEM image of weld clad interface showing thin layer of untempered martensite and $M_{23}C_6$ carbides at the interface.[4]

martensite, precipitation of $M_{23}C_6$ particles were also observed at the boundaries between the untempered martensite and ferrite. The martensite in the Figure is marked as "M" and the carbides as "C". These carbides correspond to the particles observed at the interface in the SEM image (Figure 2).

Composition variation across the interface was determined by EDS in the TEM using a 40 nm probe, Figure 4. Overall transition in composition occurred over approximately a 5 μm distance. The concentration profile was not symmetric about the interface in that the composition of the ferrite was modified for only a 1μm distance from the interface while the composition in the nickel side was modified over a larger distance (about 4μm). The asymmetry is explained based on the fact that the "interface" observed in the SEM images is a demarkation of the BCC and FCC structures and not that of "steel" and "Alloy 625". Dilution of steel with nickel at the interface region depresses the M_s temperature and converts of the original steel region to austenite causing the asymmetry.

The Alloy 625 weld consisted of columnar grains with precipitates at the grain boundaries and grain interior. SIMS images of the weld about 1mm away from the interface show that molybdenum and niobium were concentrated at the grain boundaries, Figure 5.

III.A.2. HIP Clad

Figure 6 shows SEM images of the 2¼Cr-1Mo clad in the as-received condition showing the microstructures of the base metals and the interface regions. In order to clearly describe the complex variations in microstructural features, the microstructure is partitioned into five zones, I - V. The microstructure of the steels, Region I, was comparable to the corresponding weld clad samples and consisted essentially of ferrite and tempered carbides. Region II at the interface contained a high density of precipitates which formed as semi-continuous sheets. These carbides were identified to be $(Fe_{0.6}Cr_{0.3}Mo_{0.07}Ni_{0.03})_{23}C_6$ and had the well-known Nishiyama-Wasserman orientation relationship with the ferrite matrix[4]. As described later, these carbides formed during the tempering treatment after HIP.

Region III, which had an austenite matrix, exhibited no evidence of precipitation and is referred to as the precipitate-free zone (PFZ). TEM studies revealed that only a few isolated carbides were present in this zone. The formation of PFZ has been explained as the result of enhanced carbon solubility of the Fe-based austenite in this region[4].

The PFZ was followed by a zone containing a high density of fine and coarse precipitates, region IV. The precipitates in this zone were fine at the III/IV zone interface, considerably coarser in the middle of the zone, and were again finer at IV/V zone interface. TEM studies revealed that the fine precipitates at III/IV interface ranged in size from 80 to 120 nm and formed both at grain boundaries and grain interior and were identified to be $M_{23}C_6$ carbides. The coarse precipitates in the middle of zone IV were 2 - 5μm in size and consisted of a mixture of both M_6C and $M_{23}C_6$ carbides while the fine carbides at the IV/V interface were exclusively M_6C. The density of the coarse carbides in zone IV was higher in the 4130 clad indicating the direct effect of the carbon content of the steel on the carbide density in this region.

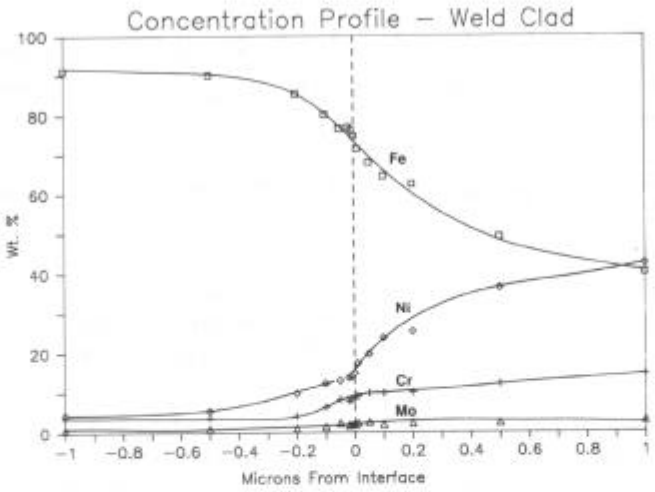

Figure 4: EDS profile of the elemental concentrations across the weld clad interface.[4]

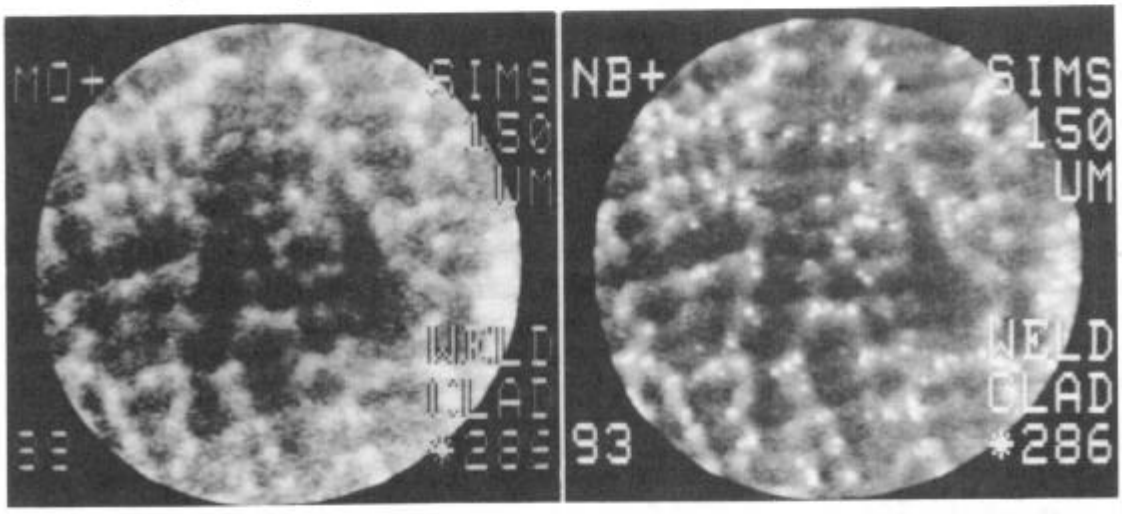

Figure 5: SIMS images of (A) Mo^+ and (b) Nb^+ in weld clad showing dendritic segregation.[4]

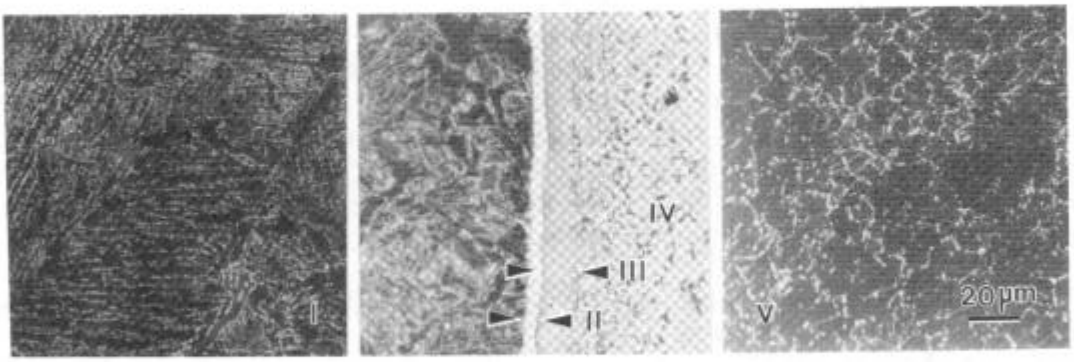

Figure 6: SEM images of HIP-clad indicating five distinct microstructural zones (I-V) at the interface.[4]

Concentration profile was also determined across the clad interface using X-ray microanalysis Figure 7. The profile shows that most of the major compositional transitions take place over a 30 μm region. As observed in the weld clad samples, the concentration profile was not symmetric about the interface and can be, again, explained as due to the conversion of the steel to austenite at the interface region.

The increased densities of carbides both in the steel and nickel sides of the interface separated by a PFZ is seemingly contrary to what would be expected. It is reasonable to assume that carbon diffuses away from the steel towards nickel and, therefore, its concentration at the interface and in Alloy 625 would be lower than in the steel bulk. In order to establish the origin of this complex distribution of carbides at the interface, the as-received HIP clad samples were heat treated to simulate the steps involved in the HIP process[4]. The analysis showed that the carbide distribution can be explained by considering both the carbon concentration and solubility gradients and a model was proposed to explain this observation, Figure 8[4].

III.B. ***Mechanical Disbond Test***:

Typical fractured specimens from the disbond tests are shown in Figure 9 where crack was allowed to propagate simultaneously in the clad and base steel. The arrows in the Figure point to the interface. Disbond was not observed in the weld samples with either base steel as evidenced by absence of secondary cracks at the steel/clad interface. Disbond was, however, observed in the HIP samples as cracks at the clad/steel interface perpendicular to the primary fracture plane. The overall extent of disbond was greatest at the clad/4130 steel interface and occurred along the dense band of carbides in Region IV of the interface as illustrated by metallographic sections of the fractured sample, Figure 10. The microhardness of the interface carbide layer exceeded 400 Vickers for the AISI 4130 base metal and was 320-380 Vickers for the 2¼Cr-1Mo steel.

III.C.***Hydrogen Disbond***:

Both UT and metallographic analysis were used to detect disbond due to hydrogen. UT inspection of the weld clad samples prior to charging detected several small indications at the bond line. Subsequent metallographic examination confirmed that these indications were caused by lack-of-fusion defects at the interface. Following charging, several large UT indications were seen at the interface and examination of metallographic sections confirmed that the indications were due to hydrogen disbond cracking at and near the clad/steel interface, Figure 11. The cracks were located primarily in the Alloy 625 weld near the clad/steel interface and propagated parallel to the interface. The extent of hydrogen disbond cracking did not appear to be influenced by the lack-of-fusion defects at the interface since cracks also occurred in some regions that did not contain the lack-of-fusion defects.

UT indications were observed at the HIP clad interface both before and after charging and were attributed to reflections from the dense carbide zone near the interface. Metallographic examination confirmed that no crack initiation occurred at the interface or along the dense band of carbides near the interface.

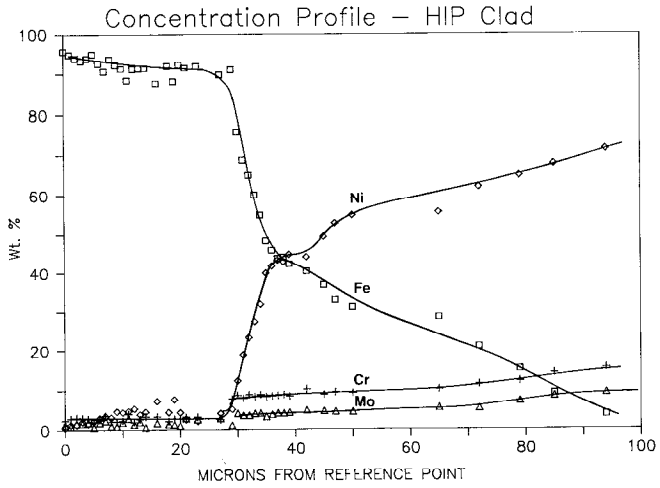

Figure 7: EDS profile of the elemental concentrations across the HIP-clad interface.[4]

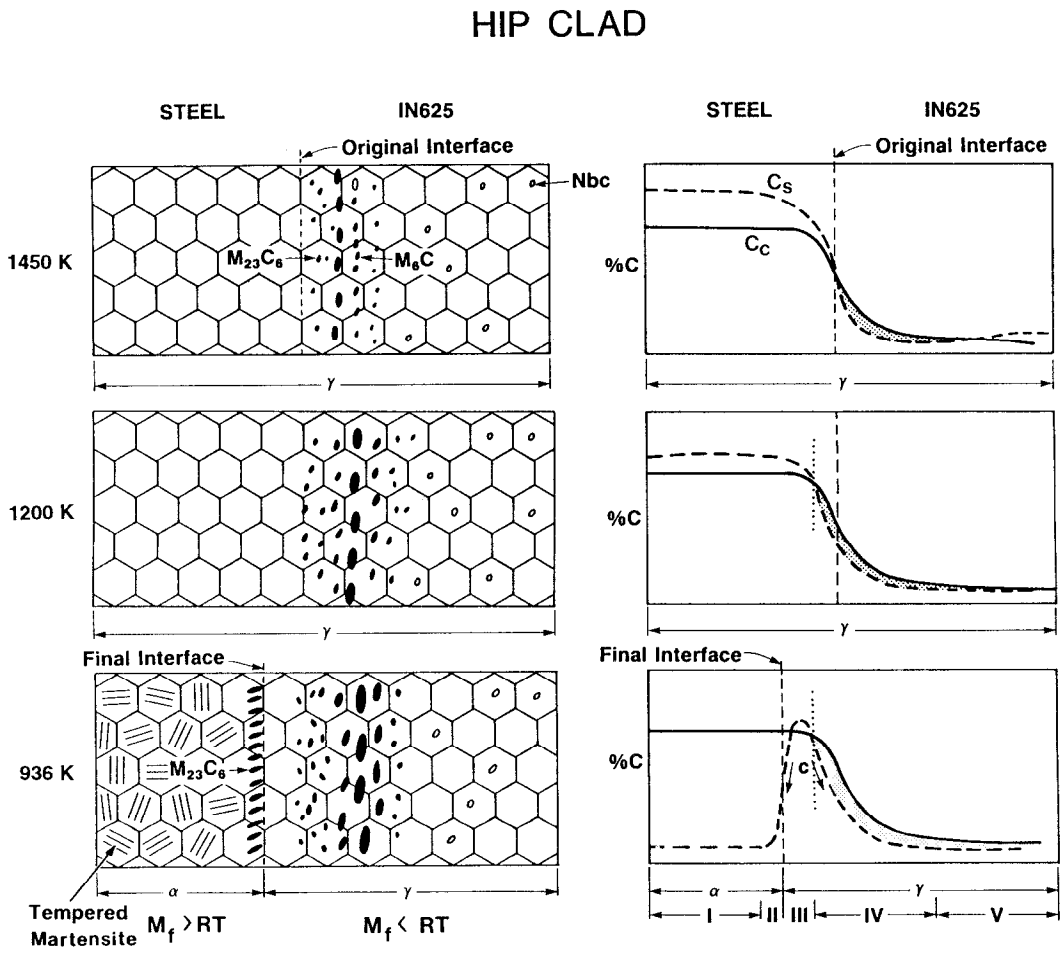

Figure 8: Schematic model illustrating evolution of the complex microstructure in the HIP-clad interface.[4]

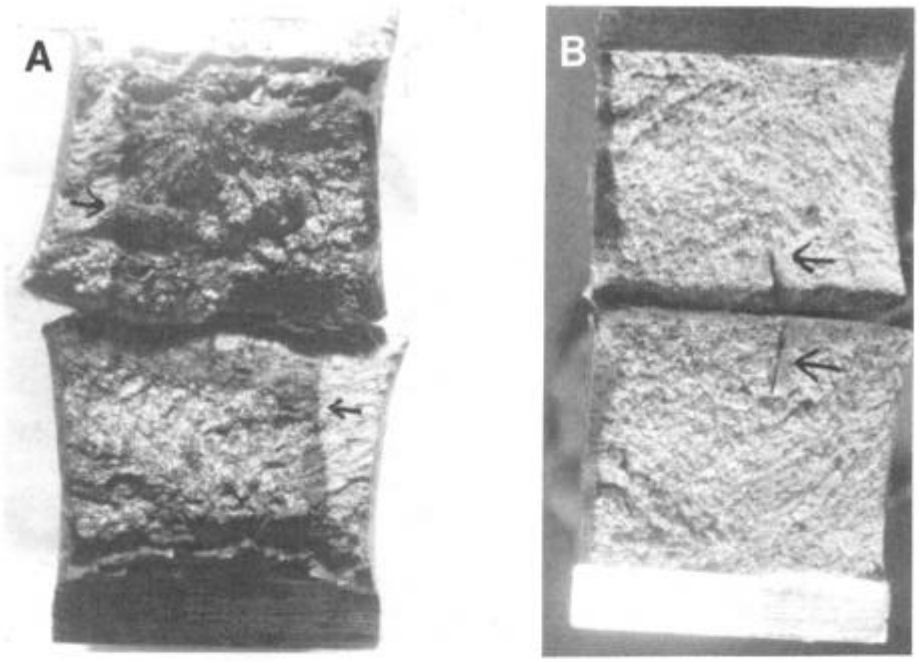

Figure 9: SEM images of fracture surfaces of Charpy samples of mechanical disbond tests in (a) Weld-clad and (b) HIP-clad.

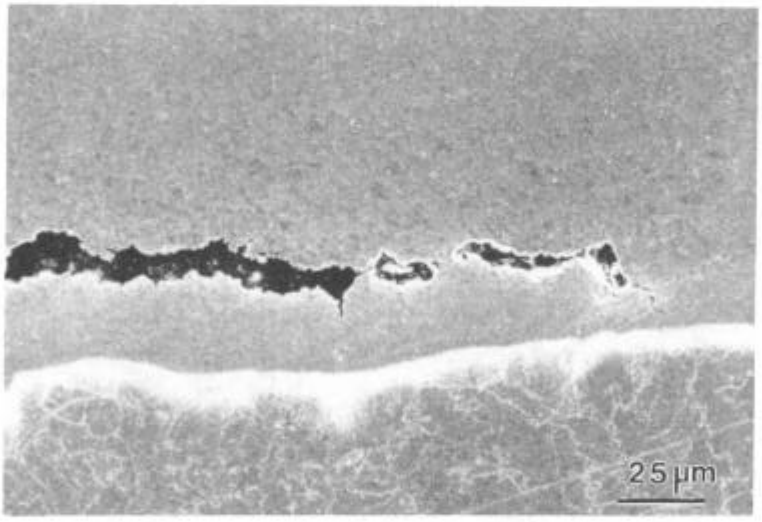

Figure 10: SEM image of polished section of HIP mechanical disbond sample showing cracks along carbide band at interface.

III.D. ***Pitting and Crevice Corrosion:***

Results of the immersion tests in the 6 WT% $FeCl_3$ and 10 WT% NaCl solution are shown in Table III. Pitting of the weld occurred at 353K. Crevice corrosion occurred at 324K, about 19K lower than the crevice threshold temperature for the HIP 625. The visual extent of corrosion of the weld 625 samples was more severe on the specimen surface removed from within 0.5 mm of the clad/steel bond line.

The HIP Alloy 625 had better resistance than weld 625 to pitting and crevice corrosion in this environment. No pitting of the HIP 625 was observed at test temperatures up to 353K. Crevice corrosion occurred at 343K. The pitting and crevice corrosion resistance of the HIP 625 were not affected by distance from the clad/steel interface.

III.E. ***Stress Corrosion Cracking***:

Positive determination of SCC in the SSRT tests requires the following: i) observation of secondary cracks or other unusual features on the gage surface of the solution tests that were not present in air tests and/or, ii) observation of a brittle fracture mode or flat, corroded zone on the fracture surface that was not present in air tests. Ratios of total elongation and/or reduction of area at fracture (RA) in the solution tests to those properties measured in air tests were calculated. The ratios, termed the embrittlement ratios, are listed in Table IV. Embrittlement ratios below 0.7 generally indicated high susceptibility to SCC.

The welded 625 cladding had good resistance to SCC at temperatures up to 450K. RA ratios were estimated for weld Alloy 625 due to non uniform gage sections in this material. Secondary cracks were observed on the gage surface at all temperatures. Subsequent metallographic examination determined that cracks at 394K and 422K were similar to secondary cracks in the air test. No SCC zones were observed on the fracture surfaces of these specimens. Secondary cracks on specimens tested at 450K were caused by SCC. Large areas of SCC were present on the fracture surfaces of specimens tested at 477, 486 and 505K.

Embrittlement ratios for HIP 625 clad were close to 1.0 for all test temperatures from 366 and 477K. Some secondary cracks were found at all test temperatures. The cracks were similar to those observed in air tests and were, therefore, not considered to be the results of SCC. A small region of SCC was observed on the fracture surface of specimen tested at 477K. SCC Fracture of both clads was associated with the formation of sulfide and oxide corrosion products on the fracture surfaces and within secondary cracks.

III.F. ***Hydrogen Embrittlement***:

The results from hydrogen embrittlement (HE) tests of Alloy 625 cladding are listed in Table V. The data show that the embrittlement ratios for weld and HIP Alloy 625 were less than 1.0. Ratios for the HIP-clad were lower than weld-clad, which indicated a higher degree of susceptibility for the HIP material. Extensive secondary cracking was observed along the gage of all of the steel-coupled tensile specimens,

TABLE IV
SCC Susceptibility of Inconel 625
from SSRT Tests

Weld Inconel 625

Temperature (K)	T_f	RA*	Comments
394	1.02	0.82	No SCC
422	0.96	1.12	No SCC on fracture surface. Some secondary cracks.
450	0.97	1.07	Secondary cracks near fracture, SCC
477	0.82	0.87	SCC, cracks in neck only.
486	0.88	0.94	SCC, secondary cracks.
505	0.69	0.94	SCC, secondary cracks

HIP Inconel 625

Temperature (K)	T_f	RA*	Comments
366	1.01	1.12	No SCC.**
394	0.94	0.88	No SCC.**
394	1.01	0.97	No SCC.**
394	1.05	0.92	No SCC.**
450	0.95	0.97	No SCC, more holes than air test.
450	0.94	0.91	No SCC.**
450	0.97	0.95	No SCC.**
477	1.06	0.93	SCC on fracture surface.

* RA values were estimated due to anisotropic deformation of weld specimens.
** Small surface defects, or holes, were present on the gauge in air and in solution tests.

TABLE V
Hydrogen Embrittlement Results for Weld- and HIP-Clad Alloy 625

Material	Test Environment	Time to Failure, t_f (hours)	RA (%)	Embrittlement Ratios t_f	RA
Weld-Clad	Air, 294 K	27.7	39.2	--	--
	Solution, 294 K	17.9	22.2	0.65	0.57
	Solution, 339 K	23.4	31.9	0.77	0.71
HIP-Clad	Air, 294K	32.8	38.9	--	--
	Solution, 294 K	9.8	12.9	0.30	0.33
	Solution, 339 K	11.2	17.2	0.34	0.44

Test Solution: 25% NaCl saturated with 15 psi H_2S, pH=2.8.

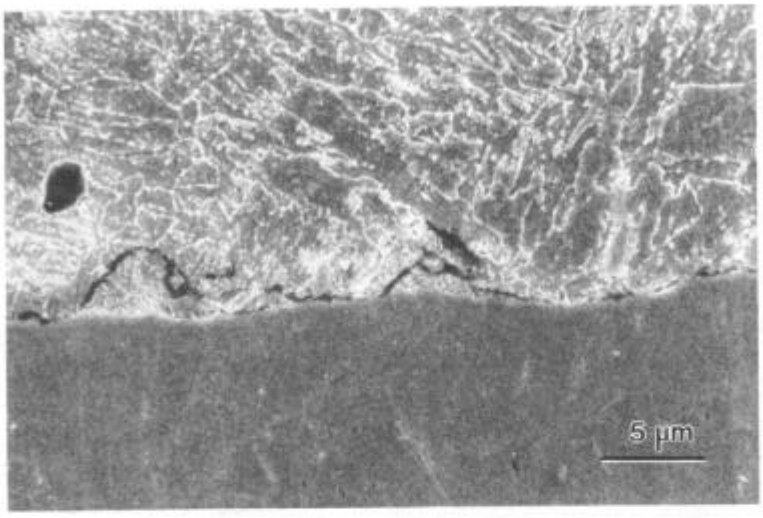

Figure 11: SEM image of cracking at weld-clad interface following hydrogen disbond test.

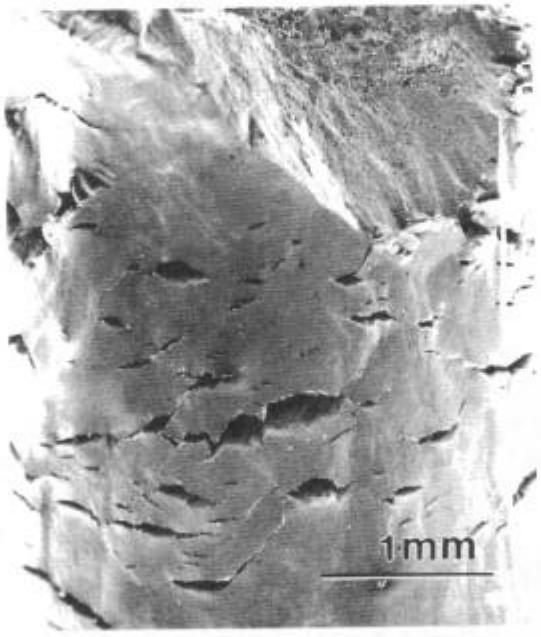

Figure 12: SEM image of HE cracks on the gauge surface of a weld-clad sample.

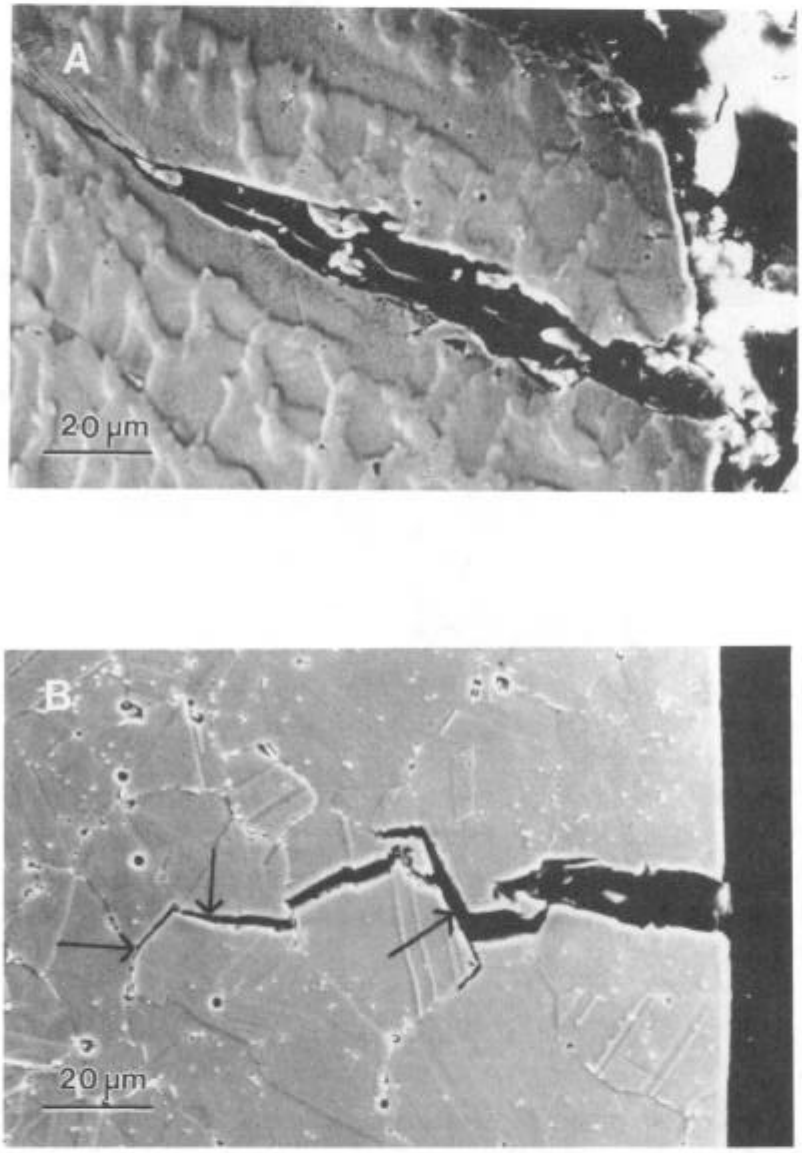

Figure 13: SEM images of metallographic sections of HE samples showing (a) interdendritic cracks in the weld-clad and (b) intergranular cracking in the HIP-clad sample.

Figure 12. Fracture surfaces of tested specimens examined in the SEM revealed multiple areas of brittle fracture were present around the edges of the fracture surfaces. These brittle regions were not present in air fractures and are, therefore, characteristic of HE fracture.

Fracture characteristics of the HE samples were examined after metallographic polishing of tested samples, Figure 13. The size and orientation of the cleavage facets in the weld clad suggested that hydrogen cracking occurred along the dendritic solidification structure. In the HIP clad specimens, fracture consisted of a mixture of intergranular and transgranular modes. Individual fractured facets were predominantly transgranular, but were separated by intergranular secondary cracks. The size and distributions of the brittle fracture facets suggested that HE cracking occurred along the grain boundaries.

IV. DISCUSSION

As mentioned earlier, a detailed elaboration of the microstructural evolution in the clad specimens is published elsewhere[4]. The following discussion primarily focuses on the relationship between the microstructure, mechanical and corrosion properties of the clads. A summary of the properties of the weld and HIP alloy is presented in Table VI.

Both the weld and HIP-clad materials formed strong metallurgical bonds at the clad/base metal interface. However, Charpy tests showed that resistance to mechanical disbond was poorer for clad made by HIP process. The disbond properties can be related to the extent of carbide precipitation in the interface region. The weld-clad interface had fewer carbides compared to HIP clad interface and, therefore, has correspondingly better resistance to mechanical disbond. The presence of thin layer of martensite in the weld clad did not seem to affect the disbond properties, presumably due to its lower carbon content compared to the bulk steel[4]. The interface of the 2 1/4Cr-1Mo steel HIP clad had better disbond resistance than that of the higher carbon AISI 4130 steel. Therefore, reduction in the carbon content of the steel should reduce carbide precipitation and improve disbond resistance.

The weld clad interface was susceptible to hydrogen disbond while the HIP clad interface was resistant to interface cracking at comparable charging current density. Hydrogen disbond cracking in the weld clad is attributed to the presence of the thin layer of untempered martensite at the interface. Internal stresses and the higher hardness of untempered martensite make this microstructure susceptible to hydrogen cracking. We were unable to prove this mechanism conclusively since direct observation of crack growth in the martensite zone is virtually impossible. If hydrogen cracks do initiate at the martensite layer, an additional stress-relief anneal should temper the martensite and improve disbond resistance.The interface defects and cracking were readily detectable using ultrasonic inspection indicating that ultrasonic inspection could be used to monitor the bond integrity of clad valves that have been in service.

The HIP-clads had better corrosion resistance than weld clads. We believe that the poorer corrosion resistance of the weld-clad 625 was caused by the

TABLE VI

SUMMARY OF MICROSTRUCTURE AND PROPERTIES

Microstructure / Properties	HIP Clad	Weld Clad
Microstructure Clad:	Homogeneous structure and equiaxed grain size	Cast, segregated grain structure
Interface:	Broad interface region (30 μm) due to extended inter-diffusion of solute elements. High density of carbide precipitation. Carbide density dependent on carbon content of steel	Relatively narrow interface zone (5μm) and fewer carbides at the interface. Thin region of untempered martensite present interface.
Mechanical Disbond	Poor	Good
Hydrogen Disbond	No interface cracking at 10mA/cm^2	Interface cracking at 10mA/cm
Pitting Corrosion (6%$FeCl_3$,10%NaCl)	Resistant up to 353K	Resistant up to 349K
Crevice Corrosion (6%$FeCl_3$,10%NaCl)	Resistant up to 343K	Resistant up to 297K
Stress Corrosion Cracking	Resistant up to 450K	Resistant up to 422K
Hydrogen Embrittlement	Intergranular Cracking	Dendritic Cracking

inhomogeneous composition of the weld deposit, which effectively resulted in a dual phase microstructure of Mo rich and Mo poor dendrites.

The HIP 625 also had better SCC resistance than the weld 625 deposits. Both clad materials exhibited good resistance in SSRT tests in acidic sour brine at temperatures up to 422K. The first indications of SCC were observed at 450K for the weld 625 and at 477 K for the HIP clad in the SSRT tests. The effect of chemical homogeneity on SCC was not evaluated in this work although it is likely that the more homogeneous composition of the HIP Alloy 625 contributed to its improved SCC resistance.

The present study shows that, when dynamically charged, both the weld and HIP clad Alloy 625 were susceptible to HE. It has been reported that dynamic charging during straining enhances hydrogen absorption at the tensile surface [6]. The net effect of the acid solution and dynamic charging is to create a high local concentration of hydrogen in the near surface region of the tensile specimen at stresses beyond yield. HE fracture occurred along grain boundary and prior particle boundaries in HIP 625 and along dendritic boundaries in weld 625. It is probable that the aging treatments during the clad process makes these boundaries susceptible sites for HE fracture. The cause of boundary fracture could be a weakening of boundary energy due to segregation of impurity elements such as phosphorous[7].

V. SUMMARY

The microstructures of Alloy 625 clad and the steel/clad interface were considerably different depending upon the type of cladding. The welded Alloy 625 clad showed classical cast structure with segregation of Mo and Nb at the grain boundaries. In contrast, Alloy 625 which was clad by HIP showed a homogeneous and equiaxed microstructure.

The interface microstructure of the clad produced by welding contained few weld defects and fewer carbide precipitates. However, a thin region of untempered martensite formed at the interface which is proposed to form during the stress relieving treatment following welding. The interface of the HIP clad composite was complex and contained two regions of dense carbide precipitation separated by a region free from any precipitation. The carbides in the Alloy 625 side of the interface consisted of $M_{23}C_6$ and M_6C particles their density was dependent on the carbon content of the steel; 4130 steel had a higher carbide density compared to the 2¼Cr-1Mo steel.

The mechanical disbond properties of the HIP clad was inferior to that of the weld clad which is attributed to the coarse and dense carbide precipitation near the interface. In contrast, disbond due the hydrogen charging was found to be inferior in the weld clad sample which has been related to the formation of untempered martensite at the interface.

HIP 625 exhibited superior corrosion and stress corrosion cracking resistance to weld overlay deposits. The differences in corrosion properties were attributed to the chemical homogeneity of HIP and weld clad deposits.

Hydrogen embrittlement in both HIP and weld 625 was associated with grain boundary fracture. The effect of post clad thermal treatments on grain boundary segregation and HE is a topic for further investigation.

REFERENCES

1. F. Matsuda, H. Nakagawa, and S. Tsuruta: Trans. J. Weld. Res. Inst., vol.15., 1986, pp. 379-80.
2. C.T. Wang and R. Hardwick: Industrial Application of Titanium and Zirconium, Race Street, Philadelphia, PA, 1984, vol. 4.
3. W.K Uhl and M.R. Pendley: Materials Performance, May 1984, pp.30-34
4. Raghavan Ayer, R.R. Mueller, D.P. Leta and W.J. Sisak: Metallurgical Transactions, vol.20A , 1989, pp.665-81
5 W.J. Sisak and J.R. Gordon: Offshore Technology Conference, Paper No.6071, Houston, TX, May 1989.
6 J.R. Scully, and P.J. Moran: Corrosion, vol. 44, No.3, 1988, p.176
7 R.D. Kane : Corrosion, vol.34, No.12, 1978, p.442